International Journal of Nanomedicine

Dovepress
open access to scientific and medical research

Open Access Full Text Article

ORIGINAL RESEARCH

Construction of a Tumor-Targeting Nanobubble with Multiple Scattering Interfaces and its Enhancement of Ultrasound Imaging

Zhengjun Ma[1], Yanmei Zhang[1], Yupu Zhu[2], Minxuan Cui[2], Yutao Liu[2], Yun-You Duan[1], Li Fan[2], Li Zhang[1]

[1]Department of Ultrasound Medicine, Tangdu Hospital, Air Force Medical University, Xi'an, People's Republic of China; [2]Department of Pharmaceutical Chemistry and Analysis, School of Pharmacy, Air Force Medical University, Xi'an, People's Republic of China

Correspondence: Li Fan; Li Zhang, Email xxfanny@fmmu.edu.cn; lilyzhang319_20@hotmail.com

Introduction: Recently, nanobubbles (NBs) have gained significant traction in the field of tumor diagnosis and treatment owing to their distinctive advantages. However, the application of NBs is limited due to their restricted size and singular reflection section, resulting in low ultrasonic reflection.

Methods: We synthesized a nano-scale ultrasound contrast agent (IR783-SiO_2NPs@NB) by encapsulating SiO_2 nanoparticles in an IR783-labeled lipid shell using an improved film hydration method. We characterized its physicochemical properties, examined its microscopic morphology, evaluated its stability and cytotoxicity, and assessed its contrast-enhanced ultrasound imaging capability both in vitro and in vivo.

Results: The results show that IR783-SiO_2NPs@NB had a "donut-type" composite microstructure, exhibited uniform particle size distribution (637.2 ± 86.4 nm), demonstrated excellent stability (30 min), high biocompatibility, remarkable tumor specific binding efficiency (99.78%), and an exceptional contrast-enhanced ultrasound imaging capability.

Conclusion: Our newly developed multiple scattering NBs with tumor targeting capacity have excellent contrast-enhanced imaging capability, and they show relatively long contrast enhancement duration in solid tumors, thus providing a new approach to the structural design of NBs.

Keywords: ultrasound contrast agents, nanobubbles, CEUS, scattering cross-section, SiO_2 NPs

Introduction

The favorable properties of nanobubbles (NBs), such as their size and ease of modification, have now been exploited to implement a theranostic platform for cancer treatment.[1–4] NB backbone-based nanotechnologies are focusing on their fabrication as an ideal tool due to their capacity for passive targeting via the enhanced permeability and retention (EPR) effect[5,6] and active targeting by functionalizing specific targeting ligands on the surfaces of NBs while transporting and controlling drug or gene delivery, thereby offering therapeutic potential.[7–10] However, when applied as ultrasound contrast agents (UCA), NBs commonly exhibit lower contrast signals compared to microbubbles due to the reduced scattering cross-section of a single bubble.[2,11,12] Efforts towards increasing the echogenicity of NBs have also been made in several studies, such as introducing a phase-change gas as the core of NBs when the NBs expand into more echogenic microbubbles under certain conditions,[13–16] or building a rattle-type mesoporous silica nanostructure with two contributing interfaces.[17,18]

Theoretically, UCA echogenicity is expressed as the sum of the scattering cross-section for a single microbubble.[19] The backscattering coefficient (BSC) can be used as a measure of the ultrasound energy scattered by the material, which correlates to the UCA echogenicity and the ultrasound contrast signal generated.[20] Studies indicate that UCA echogenicity is most dependent on the UCA size distribution and concentration.[19,21] The targeted NBs enable its enrichment and

Received: 4 February 2024
Accepted: 13 May 2024
Published: 22 May 2024

prolonged retention in tumor tissue; however, the reduction in size leads to a decrease in BSC, thereby compromising the contrast-enhanced ultrasound (CEUS) signals and accuracy compared to those achieved by microbubble contrast agents.

In our previous studies, efforts towards NB backbone-based functionalization have been made for the sake of tumor-targeted imaging and therapy.[10,22,23] Although functional elements such as anti-HER2 antibodies, IR780 or IR783 were conjugated with NB to strengthen tumor-targeted CEUS, or even to facilitate bimodal imaging as part of both CEUS and optical imaging, the NBs constructed remained limited by their barely satisfactory echogenicity when applied as UCAs for ultrasonographic diagnoses. Inspired by the structure-based design concept of enhancing cross-section scattering within a single NB, we fabricated a novel-structured NB through coating numerous hollow-structured SiO_2 nanoparticles (NPs) on their inner surfaces so as to augment the reflection interface and thus ensure active tumor-specific targeting guided by IR783. The novel-structured NBs with a "donut-type" shape could serve as a tumor-targeting UCA with enhanced echogenicity, thereby providing intensified CEUS for solid tumor imaging and suggesting widespread application in UCA-based nanobubble design.

Materials and Methods

Chemicals and Materials

We obtained methylene blue (MB) and tetraethyl orthosilicate (TEOS) from Sigma-Aldrich (St. Louis, MO, USA), while the ethanol, chloroform, and ammonia–water solution were procured from Fuyu Chemical Co., Ltd (Tianjin, China). The 1.2-distearoyl-sn-glycero-3-phosphoethanolamine-N- (methoxy (polyethylene glycol)-2000) (DSPE-PEG 2000) and 1.2-dipalmitoyl-sn-glycero-3-phosphocholine (DPPC) were purchased from Avanti Polar-lipids, Inc. (Alabaster, AL, USA), in a powdered form, and were used to fabricate NBs. IR783 were bought from Macklin (Shanghai, China) and the C_3F_8 gas of purity grade 5N was supplied by Newradar Gas Co., Ltd. (Wuhan, China). The DiO dye and Hoechst 33342 were provided by Beyotime Biotechnology Co., Ltd. (Shanghai, China). All chemical reagents were of analytical grade and were used as received without further purification.

Fabrication of IR783-SiO_2NPs@NB

To obtain the IR783-SiO_2NPs@NB, the inner layer SiO_2 NPs were first synthesized using a modified Stöber method that has been reported elsewhere.[24,25] A mixture of 75 mL ethanol and 3.4 mL 28% ammonia–water solution was prepared, and then 2.5 mg of MB (model drug molecules) was added. After adding 80 μL TEOS, the SiO_2–MB NPs were obtained by stirring for 24 hours. The NPs solution was then calcined at 550°C in a muffle furnace to remove the inner template molecules and give rise to a hollow structure. After several washes, the sample was freeze-dried for use in subsequent synthesis steps. Ultrastructural images of NPs were obtained with a transmission electron microscope (TEM) (Jeol JEM 1400 Flash, Tokyo, Japan) operating at 80 kV.

Then, the IR783- SiO_2NPs@NB was synthesized using an improved thin-film hydration method as described in our previous studies.[10,22] Briefly, 10 mg DPPC and 4 mg DSPE-PEG 2000 were mixed, and 2 mL chloroform was added to dissolve the mixture. Then, 200 μL of near-infrared fluorescent (NIRF) agent IR783 solution (dissolved in chloroform, 1 mg/mL) was added. After 10 min of rotary evaporation (120 rpm, 55°C), the chloroform was completely evaporated and formed a uniform light green phospholipid thin film. The previously synthesized SiO_2 NPs (7.5 mg) were dissolved in 1.5 mL hydration liquid (phosphate-buffered saline (PBS): glycerol = 9:1 (v/v)) and added to the bottle for film hydration, then transferred into a temperature-controlled shaker (ZWY-100D, Shanghai, China) at 130 rpm and 37°C for 60 min. The resulting suspension was divided into rubber plug tubes, which were evacuated of air and inflated with C_3F_8 gas before being oscillated for 60s in an amalgamator (HL-AH, Hangzhou, China). To prevent fluorescence quenching, the whole procedure above was performed in the dark.

Characterization of IR783-SiO_2NPs@NB

The size distribution and zeta potential of IR783-SiO_2NPs@NB were characterized using a particle size analyzer (Beckman Coulter's Delsa Nano C Particle Analyzer, Brea, CA, USA) at 25°C. The average values were obtained from three repeated measurements. Then, a drop of the diluted IR783-SiO_2NPs@NB suspension was placed on a slide

glass for examination under a fluorescence microscope (Olympus BX53F2, Tokyo, Japan) equipped with a 100× oil-immersion objective lens. Images were captured under both red fluorescence and bright field conditions. To further investigate the structure of IR783-SiO_2NPs@NB, scanning electron microscopy (SEM) (Hitachi S4800, Tokyo, Japan) was applied. All samples were air-dried at room temperature before being coated with a layer of gold on their surfaces. Meanwhile, we synthesized NBs without inner layer NPs, termed IR783-NB, as controls.

Determining the Efficiency of Encapsulation (EE) of IR783 in IR783-SiO_2NPs@NB

The concentration of IR783 in IR783-SiO_2NPs@NB was quantified using a standard curve, which was established by measuring the spectra of different concentrations of IR783 with a spectrophotometer (Biotek SYNERGY LX, Wichita, KS, USA). IR783-SiO_2NPs@NB was separated from the original solution by centrifugation (1500 rpm, 5 min) at 4°C to remove the fragmented liposome membrane and IR783 that not loaded on NBs. After that, IR783-SiO_2NPs@NB and all the agents including IR783, DPPC, DSPE-PEG 2000, and SiO_2 NPs were dissolved in ethyl alcohol. The EE of IR783 were calculated as follows:

$$\mathrm{EE}(\%) = \frac{\text{weight of IR783 in IR783} - \mathrm{SiO_2NPs@NB}}{\text{weight of total added IR783}} \times 100\%$$

Evaluating the Stability and Cytotoxicity of IR783-SiO_2NPs@NB

The stability of IR783-SiO_2NPs@NB was evaluated by monitoring changes in particle size and concentration over time. The diluted IR783-SiO_2NPs@NB sample was added in droplet form onto a hemocytometer and assessed using a fluorescence microscope to determine the concentration. The particle size and concentration were measured at 1, 15, 30, 45 and 60 min at 25°C after fabrication, and the procedures were repeated three times. The cytotoxicity of IR783-SiO_2NPs@NB on VX2 cells in vitro was evaluated using the Cell Counting Kit-8 (CCK-8) (ZETA LIFE, Menlo Park, CA, USA), as follows. The VX2 cells, derived from rabbit hepatocellular carcinoma cell line and obtained from Sunncell Biotech (Wuhan, China), were seeded at a density of 5×10^3 cells per well in a 96-well plate and cultured for 12 hours until they adhered to the bottom surface. Subsequently, the cells were exposed to IR783-SiO_2NPs@NB at various concentrations (ranging from 1.9×10^6 to 5×10^8 /mL) in fresh medium for 24 hours, followed by treatment with CCK-8 reagents (10 μL) for 2 hours. The absorbance was recorded at 450 nm using the spectrophotometer.

Assessing the Tumor Specific Binding Efficiency of IR783-SiO_2NPs@NB

NBs labeled with 5 μL of DiO dye (DiO-SiO_2NPs@NB) served as the control group. The VX2 cells were trypsinized and equally distributed into two 20 mm confocal dishes. The first dish was treated with 100 μL DiO-SiO_2NPs@NB (5×10^6 /mL), and the second dish was treated with 100 μL IR783-SiO_2NPs@NB (5×10^6 /mL). The two dishes were incubated at 37°C for 2 hours, followed by gentle washing with 1× PBS three times. After 10 min of incubation with Hoechst 33342 to stain the cells' nucleus, fluorescence images were captured using a confocal laser scanning microscope (CLSM) (Carl Zeiss LSM 800, Oberkirchen, Germany) with a ×20 objective lens. The specific binding efficiency of IR783-SiO_2 NPs@NB towards VX2 cells was analyzed on a CytoFLEX S flow cytometer (Beckman Coulter, Brea, CA, USA). The cells were treated in the same manner as above, and all procedures were repeated thrice under dark conditions using aluminum foil.

Measuring the Echogenicity of IR783-SiO_2NPs@NB in vitro

The echogenicity of IR783-SiO_2NPs@NB was investigated using the fingertip of a latex glove containing diluted NBs immersed in a water bath. PBS was set as the negative control and commercially available sulfur hexafluoride microbubbles SonoVue (Bracco, Milan, Italy) were used as the positive control group. All the NBs/NPs were diluted with 1× PBS to the same volume and concentration (10 mL, 5×10^5 /mL). The in vitro echogenicity changes of NB, IR783-NB and IR783-SiO_2NPs@NB were compared over a 60-min period. Gray scale and CEUS images were acquired using a Mindray Ultrasound System (Resona 7, Shenzhen, China) with a linear array transducer set to a frequency of 5.6

MHz and a mechanical index (MI) of 0.086. The analysis of the mean brightness value of CEUS images in each group (n = 5) was performed using Image J software (version 1.53s).

Establishing Mouse Xenograft Models

Athymic nude mice (male BALB/c, 6–8 weeks old) were kept under SPF conditions in our own facilities. To establish the mouse xenograft model, VX2 cells (1×10^7) suspended in 100 μL 1× PBS were subcutaneously injected into the right flank of each nude mouse. Tumors were allowed to grow in 2 weeks.

Measuring the CEUS Imaging Ability of IR783-SiO_2NPs@NB in vivo

The in vivo CEUS imaging ability was assessed in the tumor-bearing nude mice, and the mice were randomly divided into five groups (n = 6 per group). Initially, the nude mice were anesthetized with 1% isoflurane via inhalation and immobilized on a tray table prior to ultrasonic imaging. Tumor CEUS images were acquired using a linear array transducer operating at a frequency of 4.7 MHz and MI of 0.086 in contrast-enhanced mode. The negative control group received an intravenous administration of 100 μL PBS, while the other groups were administered NB, SonoVue, IR783-NB or IR783-SiO_2NPs@NB in equal quantities (100 μL, 1×10^6 /mL) via the caudal vein. The region of interest (ROI) for all images was defined as the tumor area, excluding regions without contrast agent perfusion. The time of video recording was set as the first bubble appeared in ROI. The total cine acquisition time was 3 min and the time–intensity curve (TIC) was analyzed automatically using the quantitative analysis software package in Resona 7 after CEUS. TTP was defined as the time to peak intensity measured from the TIC. PI was the peak intensity assessed by TIC. Image J software (version 1.53s) was used for the analysis of the mean brightness value of the CEUS images, and the area under the curve (AUC) was calculated and analyzed using GraphPad Prism (version 8.0.1).

Determining the Biodistribution and Biosafety of IR783-SiO_2NPs@NB

Two days after CEUS, the accumulation of IR783-SiO_2NPs@NB in VX2 tumors was visualized using an in vivo fluorescence imaging system (IVIS Lumina II, Caliper, MA, USA). Specifically, 100 μL of the IR783-SiO_2NPs@NB (1×10^6 /mL) was administered via caudal vein injection, and observation was undertaken using the IVIS system 1 hour later. To evaluate the biodistribution and metabolism of IR783-SiO_2NPs@NB in vivo, nude mice were administered with the same dose as described above. At 1, 6, and 24 hours after administration, the mice were sacrificed and their tumors and major organs were harvested for NIRF imaging using the IVIS system.

The Biosafety Assessment of IR783-SiO_2NPs@NB

After conducting the above-mentioned experiments, nude mice were anesthetized and subsequently euthanized via cervical dislocation. Heart, kidney, liver, spleen, and lung samples were then isolated and prepared for paraffin-embedding. Following deparaffinization, hematoxylin and eosin (H&E) staining was performed on the sections which were subsequently observed under an optical microscope (Nikon Ci-s, Tokyo, Japan).

Statistical Analysis

One-way analysis of variance (ANOVA), followed by Tukey post hoc multiple comparison tests, was performed in GraphPad Prism (version 8.0.1). The data are presented as means ± standard deviation (SD), and statistical significance was determined at a level of $p \leq 0.05$.

Results

Characteristics and Morphology of SiO_2 NPs

The SiO_2 NPs, prepared according to the method described in 2.2, are shown in Figure 1A. The freshly prepared nanosuspension exhibited a translucent appearance, and a clear Tyndall effect could be observed upon illumination with a red laser beam, indicating that the SiO_2 NPs were well dispersed and homogeneous (Figure 1B). The TEM images depict the SiO_2 NPs before (Figure 1C) and after calcination (Figure 1D), exhibiting a spherical morphology with an average diameter of ~80 nm. After calcination, the NPs displayed a hollow spherical structure.

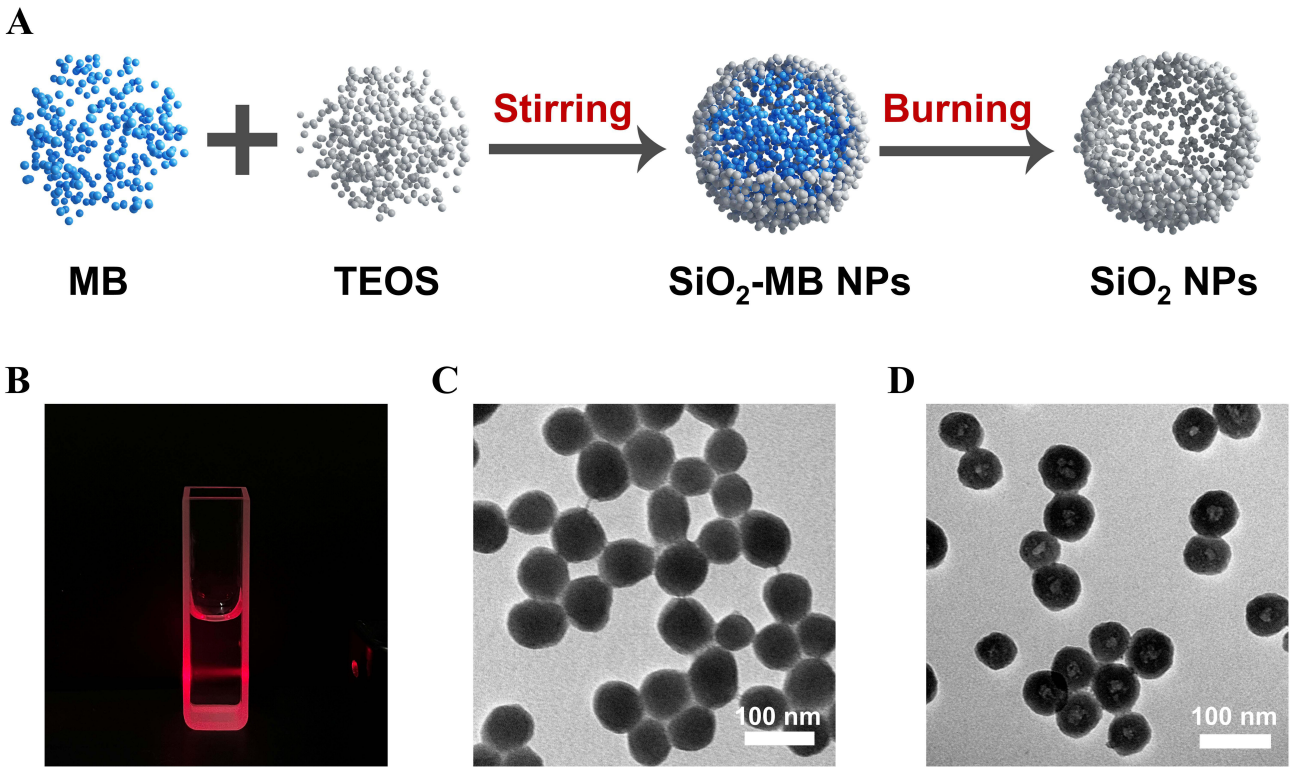

Figure 1 Characteristics and morphology of SiO_2 NPs.
Notes: (**A**) Schematic illustration of the synthesis of SiO_2 NPs. (**B**) Aqueous solution of SiO_2 NPs illuminated by a red laser. TEM images of SiO_2 NPs before (**C**) and after (**D**) calcination.

Characteristics and Morphology of IR783-SiO_2NPs@NB

The IR783-SiO_2NPs@NBs were successfully synthesized using the improved thin-film hydration method, as illustrated in Figure 2A. The mean diameter and zeta potential of IR783-SiO_2NPs@NB were approximately 637.2 ± 86.4 nm and −29.5 ± 0.9 mV, respectively (n = 3) (Figures S1A and S1B). In comparison, the average particle size and zeta potential of the IR783-NB, serving as the control group, were measured to be 583.6 ± 107.7 nm and −23.8 ± 5.2 mV, respectively (n = 3) (Figures S1C and S1D). The morphology of IR783-SiO_2NPs@NB served as the reference and was observed under bright field using a 100× oil-immersion objective lens. Upon laser excitation at a wavelength of 640 nm, numerous nano-sized bubbles exhibited NIRF emissions against a dark-field background (Figure 2B), confirming the successful encapsulation of IR783 within NBs and the potential of NIRF imaging to visualize IR783-SiO_2NPs@NB. The IR783-SiO_2NPs@NB exhibited a "donut-type" structure, as shown in Figure 2C under SEM scanning, while the IR783-NB only showed a nano-scale hollow spherical structure (Figure 2D).

IR783 Loaded in IR783-SiO_2NPs@NB

The absorption spectra of different concentrations of IR783 exhibited a prominent peak at 786 nm, as depicted in Figure S2A. In contrast, DPPC, DSPE-PEG 2000, and SiO_2 NPs displayed negligible absorbance within the wavelength range of 400 nm to 1000 nm. Upon loading with IR783, IR783-SiO_2NPs@NB demonstrated an unaltered absorption peak at 786 nm, consistent with that of free IR783 (Figure S2B). After conducting three repeated experiments and calculations, the EE of IR783 in IR783-SiO_2NPs@NB was determined to be 15.4 ± 1.9%.

Cytotoxicity and Stability of IR783-SiO_2NPs@NB

As Figure 3A shows, the average size of IR783-SiO_2NPs@NB at 30 min did not change significantly when compared with the size at 1 min (877.5 ± 107.9 nm vs 637.2 ± 114.0 nm, $p = 0.132$) in room temperature. The NBs then coalesced to form larger bubbles with time. At 45 min, the average size of IR783-SiO_2NPs@NB increased to 1014.3 ± 140.6 nm, which was significantly bigger than the initial size at 1 min ($p < 0.05$). Similar results were observed as the concentration

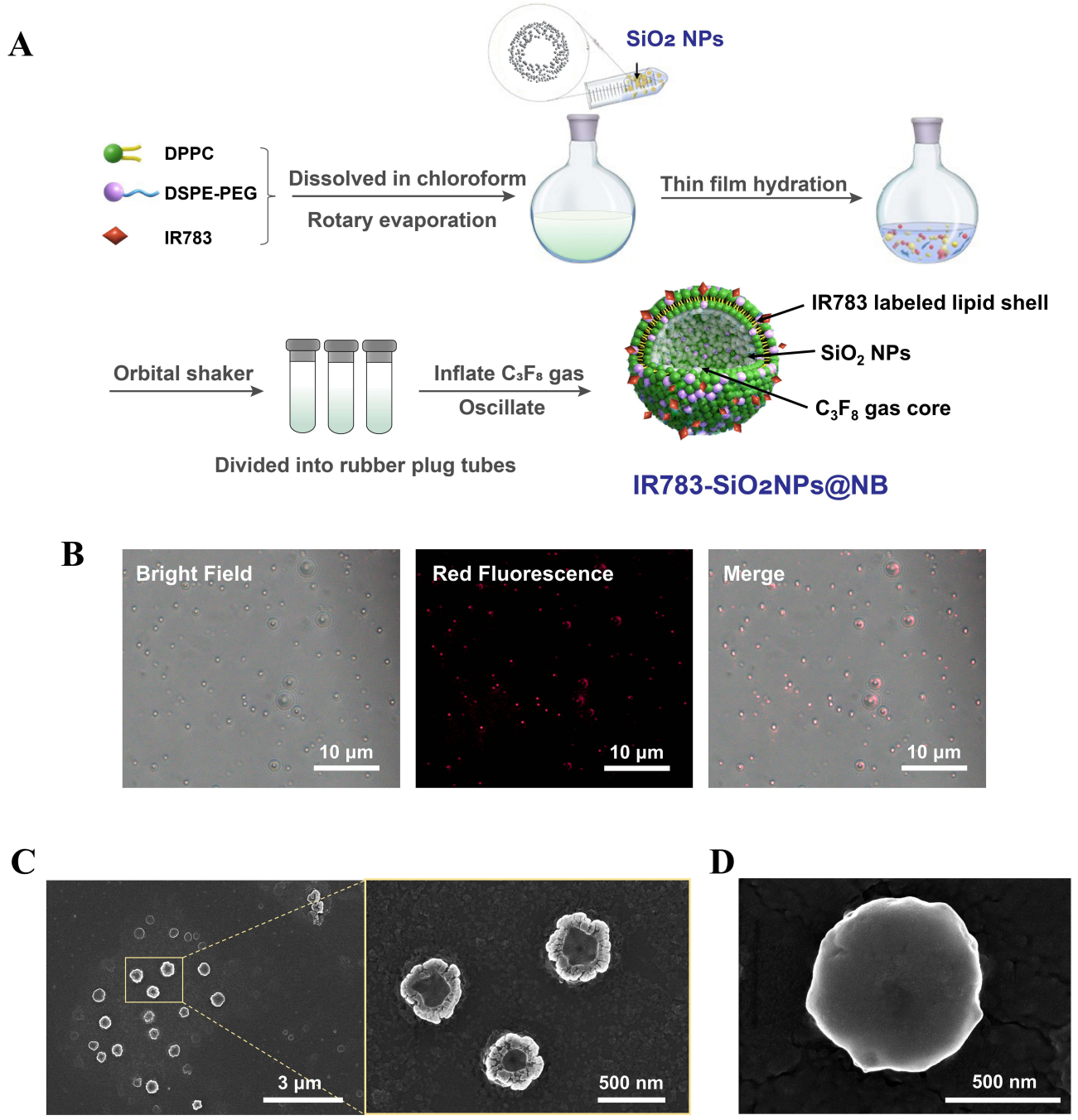

Figure 2 Characteristics and morphology of IR783-SiO_2NPs@NB.
Notes: (**A**) Schematic illustration of the synthesis of IR783-SiO_2NPs@NB. (**B**) Bright field and NIRF microscopy image of IR783-SiO_2NPs@NB with 100× oil-immersion lens. SEM image of IR783-SiO_2NPs@NB (**C**) and IR783-NB (**D**).

of NBs was evaluated. The concentration of IR783-SiO_2NPs@NB remained stable over a 45-min period, as Figure 3B shows. At 60 min, there was a noticeable decrease in the NB concentration ($11.5 \pm 1.2\times10^6$ /mL) when compared with the initial concentration of $17.8 \pm 1.1\times10^6$ /mL. The maximal time interval over which the IR783-SiO_2NPs@NB remained stable, 30 min, is good enough to fulfill the requirements of ultrasound imaging with in vivo application.

The cell survival rate curve was obtained using the CCK-8 assay (Figure 3C). The statistical analysis revealed that there was no significant cytotoxicity when the concentration range of IR783-SiO_2NPs@NB remained within 5×10^8 /mL.

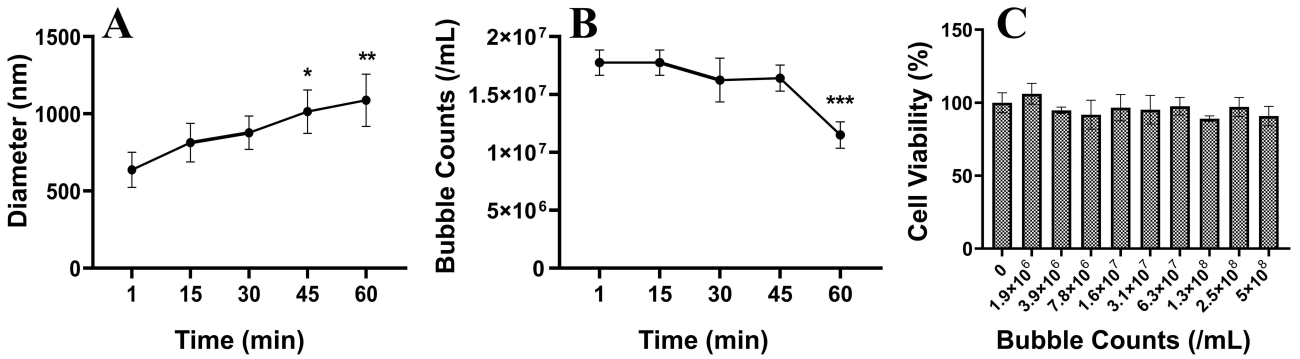

Figure 3 The diameter (**A**) and the concentration (**B**) of IR783-SiO_2NPs@NB changes over time at 25°C. (**C**) The cytotoxicity for various concentrations of IR783-SiO_2 NPs@NB determined using the CCK-8 assay.
Note: (**A** and **B**) *p <0.05, **p <0.01, and ***p <0.001 indicate statistically significant differences compared with those observed at 1 min.

Tumor Specific Binding Efficiency of IR783-SiO_2NPs@NB in vitro

The results show that the IR783-SiO_2NPs@NB group exhibited a significantly high NIRF signal in the hepatocellular carcinoma VX2 cells (Figure 4A), with a remarkably high proportion of stained cells reaching 99.78% (Figure 4B). In contrast, the DiO-SiO_2NPs@NB group (control group) displayed little or no NIRF signal within the VX2 cells (Figure 4A), and only a negligible proportion of stained cells was observed at 0.14% (Figure 4C).

Echogenicity of IR783-SiO_2NPs@NB in vitro

The in vitro echogenicity of IR783-SiO_2NPs@NB was verified via an analytical setup (Figure 5A). Compared with the negative control PBS, SiO_2 NPs exhibited discernible echogenicity with a brightness value of 20.63±5.60, which was much lower than that of NBs, as shown in Figure 5B. The NB (121.05±7.94) and IR783-NB (115.05±4.74) presented similar echogenicity values in vitro (p = 0.807), but these were much lower than that of SonoVue (147.13±13.54, p = 0.0002 and p < 0.0001). The mean brightness value of IR783-SiO_2NPs@NB (162.04±6.18) was higher compared to

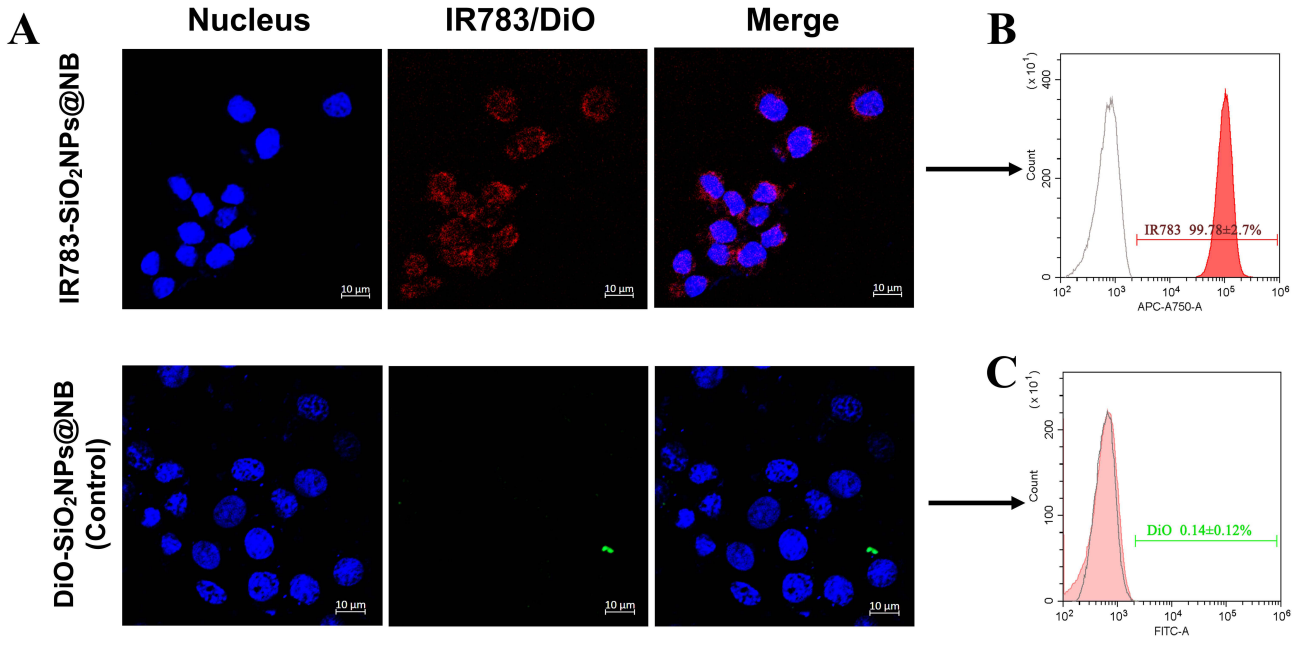

Figure 4 The tumor specific binding efficiency of NBs was evaluated by co-incubation with VX2 cells in vitro.
Notes: (**A**) The CLSM images of VX2 tumor cells incubated with IR783-SiO_2NPs@NB (up) and DiO-SiO_2NPs@NB (down) for 2 hours. Bar, 10 μm. The specific binding efficiency of IR783-SiO_2NPs@NB (**B**) and DiO-SiO_2NPs@NB (**C**) for VX2 cells determined via FCM analysis.

https://doi.org/10.2147/IJN.S462917 DovePress

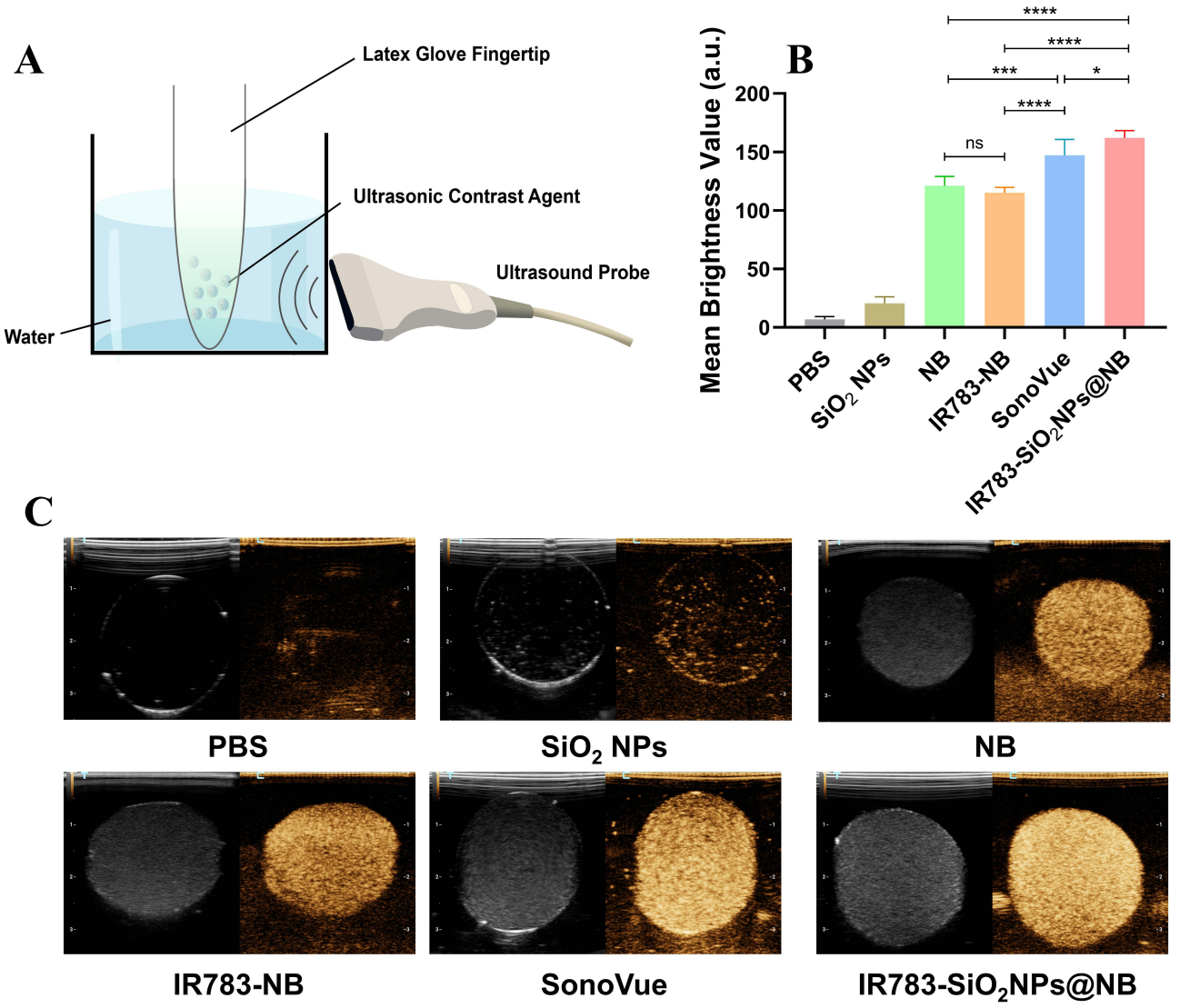

Figure 5 Evaluation of echogenicity of IR783-SiO_2NPs@NB in vitro.
Notes: (**A**) Schematic illustration of the device used for ultrasound imaging in vitro. (**B**) Statistical analysis of the mean brightness values of images under contrast mode (ns = not significant, *$p < 0.05$, ***$p < 0.001$, ****$p < 0.0001$). (**C**) Comparison of the CEUS imaging capacity in vitro. A consistent bubble concentration (5×10^5 /mL) was maintained for each group throughout the experiment.

those of IR783-NB ($p < 0.0001$), NB ($p < 0.0001$) and SonoVue ($p = 0.0475$). The above results are in accordance with the visual observations; Figure 5C shows that when compared with the SonoVue microbubbles at an equivalent bubble concentration under CEUS mode, NB and IR783-NB demonstrated inferior contrast-enhancing capabilities, while IR783-SiO_2NPs@NB appeared much brighter. The echogenicity of NB, IR783-NB, and IR783-SiO_2NPs@NB changes with time for a duration of 1 hour, as depicted in Figure S3. These contrast agents remain stable during the initial 30-minute period.

Contrast Enhancement Ability of IR783-SiO_2NPs@NB in vivo

After xenograft models of nude mice with tumor size of 1.808 cm/1.518 cm were constructed (Figure 6A), gray scale and color Doppler ultrasound images were obtained to measure the tumor size and evaluate the blood supply in the tumor (Figure 6B). As Figure 6C indicates, with the exception of the negative control group treated with PBS, all NBs were washed in the tumor and delineated the tumor's boundary after bubble injection, as SonoVue did; all NBs exhibited a good enhanced contrast imaging ability within the first 10s. However, the NB group was washed out quickly, and the

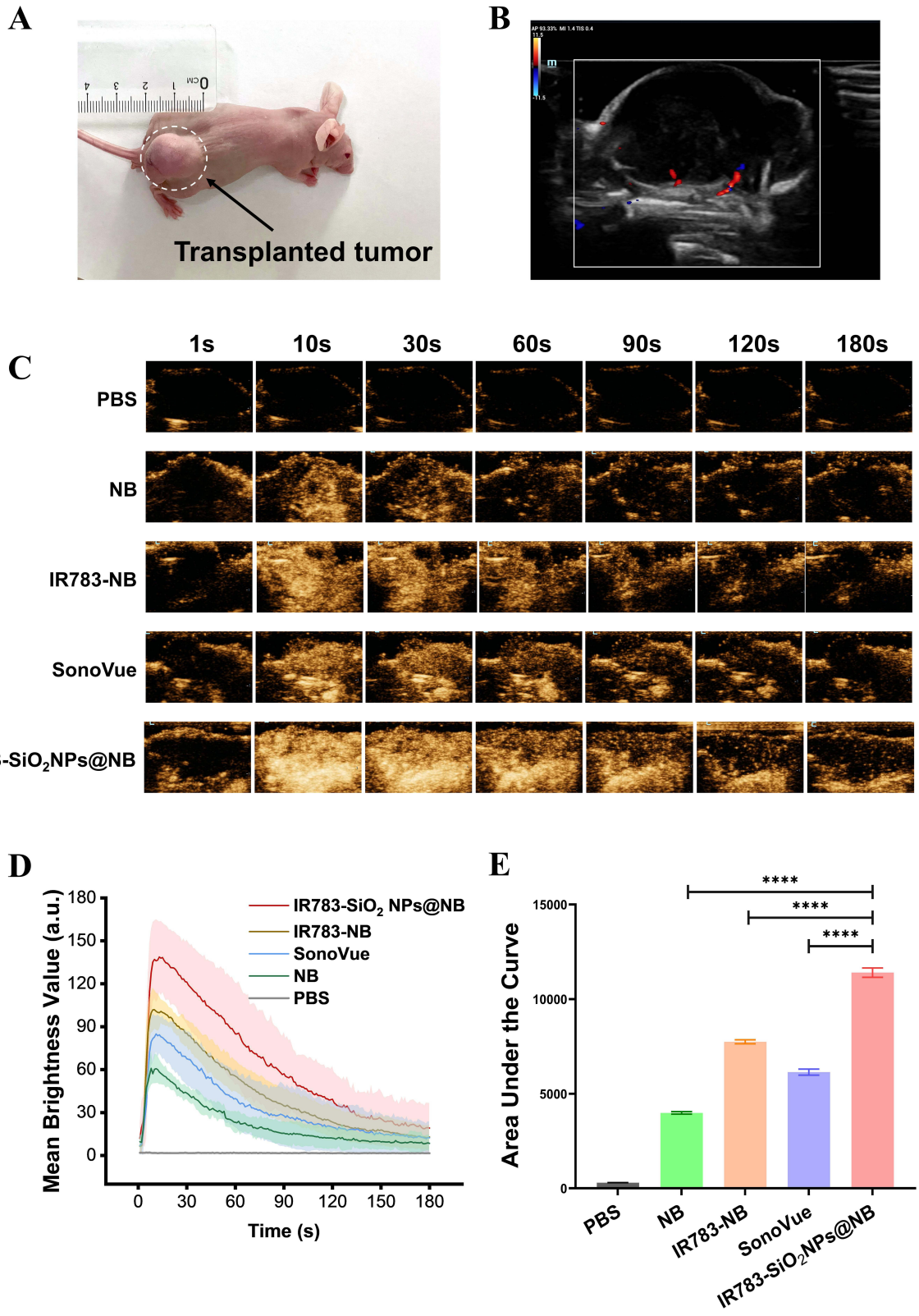

Figure 6 Evaluation of the CEUS imaging capacity of IR783-SiO_2NPs@NB in vivo.

Notes: (**A**) VX2-transplanted tumor in nude mouse model. (**B**) Color Doppler ultrasound image of VX2 tumor (in white frame). (**C**) CEUS imaging of tumor after injection of PBS, NB, IR783-NB, SonoVue, or IR783-SiO_2NPs@NB at various time points (1, 10, 30, 60, 120, and 180 s). (**D**) TIC and its confidence bands for NB, IR783-NB, SonoVue, or IR783-SiO_2NPs@NB. (**E**) AUC analysis with data extracted from Figure 6D (****$p < 0.0001$).

tumor presented as hypoechoic at 30s, as compared with others. When comparing the contrast enhancement ability with SonoVue, both IR783-NB and IR783-SiO_2NPs@NB demonstrated comparatively long retention times in the tumor, and that the contrast enhancement within tumors provided by IR783-NB and IR783-SiO_2NPs@NB remained significantly superior to that provided by SonoVue at both 60s and 90s. The contrast-enhanced differences between IR783-NB and IR783-SiO_2NPs@NB were visually indistinguishable.

TIC revealed the changes in intensity in the tumor with time, as shown in Figure 6D. The profile shows a rapidly rising slope from the time of the bolus injection to the PI, and a gradually descending slope after reaching PI, for all UCAs. Further statistical analyses of the UCAs' perfusion parameters verified that there was no significant difference in TTP values among these UCAs, which were all around 10s to 12s (Table 1). The highest PI at TTP, 142.27±23.37, was obtained by the IR783-SiO_2NPs@NB group, which is significantly higher than the values achieved by NB, IR783-NB and SonoVue (Table 1). To further compare the contrast enhancement capacities of the UCAs as a function of imaging time, AUC plots for the UCAs from washing in to washing out were created and statistically analyzed. The results show that the enhancements achieved by IR783-SiO_2NPs@NB (11,401±245.9) were significantly stronger than the enhancements induced by the SonoVue (6143±161.8), NB (3987±65.17) and IR783-NB (7747±103.2) ($p < 0.0001$; Figure 6E). The contrast signal intensity of IR783-SiO_2NPs@NB was maintained at a significantly higher level at 60s and 90s with respect to that of SonoVue, whereas IR783-NB only presented stronger signals than NB at these two time points (Table 2).

Tumor Tissue Accumulation, Bio-Distribution, and Biosafety in vivo of IR783-SiO_2 NPs@NB

As depicted in Figure 7A, equivalent volumes of saline and IR783-SiO_2NPs@NB were respectively administered via the tail vein of nude mice bearing VX2 tumors. After 1-hour, notable fluorescence accumulation could be observed, specifically within the tumor tissue in the IR783-SiO_2NPs@NB group, while no fluorescence signal was detected in

Table 1 Comparison of TTP, PI, and AUC for TIC of NB, IR783-NB, SonoVue, and IR783-SiO_2NPs@NB in vivo

	NB	IR783-NB	SonoVue	IR783-SiO_2NPs@NB
TTP (s)	9.67±3.27	10.00±2.68	11.17±2.40	12.50±1.87
PI (a.u.)	63.59±9.85	106.84±9.50[a]	88.15±14.24	142.27±23.37[a,b,c]
AUC	3987±65.17	7747±103.2[a,c]	6143±161.8[a]	11,401±245.9[a,b,c]

Notes: Data are presented as means ± SD. [a]Statistical difference compared to NB; [b]Statistical difference compared to IR783-NB; [c]Statistical difference compared to SonoVue. Statistical difference is indicated by a *p*-value of less than 0.05.
Abbreviations: TTP, time to peak intensity; PI, peak intensity; AUC, area under the curve.

Table 2 Comparison of Mean Brightness Values Derived from CEUS Images of NB, IR783-NB, SonoVue, and IR783-SiO_2NPs@NB in vivo

Time	NB	IR783-NB	SonoVue	IR783-SiO_2NPs@NB
1 s	7.34±4.30	7.07±4.76	9.87±7.17	9.06±6.04
10 s	57.23±10.75	99.68±14.86[a]	88.27±14.04[a]	127.95±14.54[a,b,c]
30 s	44.73±9.64	86.10±10.14[a,c]	68.42±18.99[a]	105.59±14.36[a,b,c]
60 s	26.95±9.36	59.15±12.21[a]	44.74±18.23	74.81±17.82[a,c]
90 s	19.45±7.28	39.52±14.43[a]	30.34±18.36	50.96±17.92[a,c]
120 s	13.02±7.66	30.30±13.50	22.21±15.98	34.16±16.71[a]
180 s	9.39±7.85	16.62±9.15	12.96±14.30	17.02±11.04

Notes: Data are presented as means ± SD. [a]Statistical difference compared to NB; [b]Statistical difference compared to IR783-NB; [c]Statistical difference compared to SonoVue. Statistical difference is indicated when the *p*-value is less than 0.05.

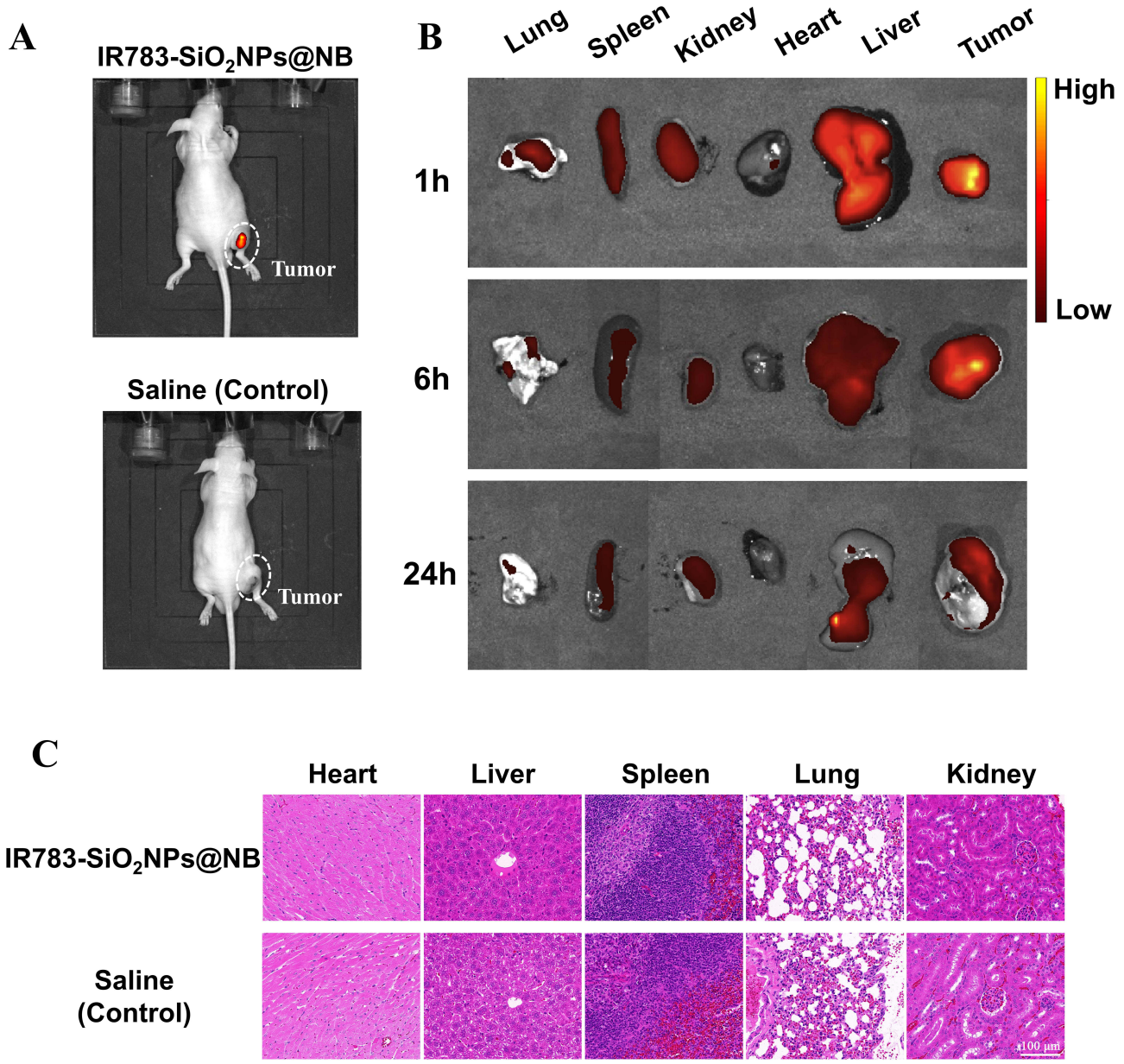

Figure 7 (**A**) The in vivo tumor tissue accumulation of IR783-SiO_2NPs@NB (up) and saline (down) at 1 hour evaluated by NIRF imaging. (**B**) Ex vivo fluorescence imaging of the lung, spleen, kidney, heart, liver, and tumor at different time points after IR783-SiO_2NPs@NB injection. (**C**) H&E staining was conducted on heart, kidney, liver, spleen, and lung sections of nude mice injected with IR783-SiO_2NPs@NB (up) and saline (down).
Note: (**A**) The white dotted circles indicated the tumors.

the saline group, suggesting the tumor-specific targeting capacity of IR783-SiO_2NPs@NB. To further confirm the biodistribution and metabolism of IR783-SiO_2NPs@NB in vivo, a tissue fluorescence imaging experiment was conducted. Fluorescent signals derived from the lung, spleen, kidney, heart, liver, and tumor of nude mice were analyzed at different time points after injection (Figure 7B). The results demonstrate that, following the administration of IR783-SiO_2NPs@NB, relatively high fluorescence intensity developed in the tumor and liver, which gradually decreased over time. Conversely, the spleen, kidney, and lung exhibited consistently low levels of fluorescence signal, with almost negligible fluorescence signals observed in the heart. The histological changes in major organs in each group were examined using H&E staining (Figure 7C). No significant alterations were observed in the heart, kidney, liver, spleen, or lung among the two groups. The results demonstrate that IR783-SiO_2NPs@NB exhibited negligible detrimental effects on the major organs of nude mice, thereby substantiating its high degree of biological safety.

Discussion

The newly constructed IR783-SiO_2NPs@NB presented in this paper comprised a phospholipid shell conjugated with tumor-targeting moiety IR783 on its surface, containing C_3F_8 in the inner core and a certain amount of SiO_2 NPs on the inner surface, showing a similar structure to a donut. The IR783-SiO_2NPs@NB performed much better in CEUS imaging, as was embodied in both the much higher echogenicity and much longer retention time in the tumor, which has been attributed to the "donut-type" structure. In general, as a nano-metric of UCA, the reasons favoring its accumulation and retention in the tumor at comparatively high concentrations are as follows: i) its extravasation into the tumor due to the passive tumor-targeting effect via EPR at a size of ~600 nm size; ii) its active tumor-targeting capacity, as indicated by the inherent cancer-targeting ability of IR783; iii) the multiple scattering/reflection interfaces provided by SiO_2 NPs magnified the echo signal compared to hollow nanostructures with only one interface; iv) the SiO_2 NPs released when some bubbles burst were capable of playing the role of an ultrasound imaging medium.

Interestingly, the in vitro results indicate that the echogenicity of IR783-NB was similar to that of NB, and those of both IR783-NB and NB were lower than that of SonoVue, which differs from the results of in vivo experiments. The CEUS imaging capacity of IR783-NB in the tumor improved greatly after the bubble suspension was injected into the mice carrying a tumor, indicating that the inherent cancer-targeting ability of IR783 played a pivotal role in the CEUS imaging capacity by increasing the concentration of bubbles when applied in vivo. Several studies have reported that ligand-modified NBs universally displayed a better contrast-enhancing effect or facilitated a longer imaging time than unmodified MBs in multiple tumor models,[23,26,27] which has been confirmed by our results that IR783-NB performed even better than SonoVue at the given imaging resolution and duration. IR783 offered a strong tumor-binding ability with a 99.78% tumor specific binding efficiency, allowing it to drag more bubbles into the tumor tissue and thus produce a higher brightness value and longer retention time. On the other hand, without the help of active targeting moiety, the performance of NBs was mediocre when depending only on the passive tumor-targeting effect via EPR.

Although the targeted NBs enable tumor tissue enrichment and a long retention time, the reduction in size leads to a decrease in nonlinear backscattering, thereby weakening the CEUS imaging capacity and compromising imaging accuracy compared to microbubble contrast agents.[4,19] However, the previously reported UCAs all shared the same structure, with only one contributing interface, and thus they can only realize scattering/reflection once in ultrasound imaging as a result of their structure, leading to the limited utilization of ultrasound waves. The scattering cross-section plays a crucial role in CEUS efficacy. According to the Rayleigh scattering law,[28] at a constant ultrasonic frequency, the scattering cross-section is solely determined by the scattering radius; thus, larger total scattering radii result in larger scattering cross-sections and stronger ultrasonic signals being received. For UCAs with the same composition but different structures, the ratio of single scattering to incident ultrasound is lower than that of twice (or more) scattering to incident ultrasound in a single NP. Zhang developed a "rattle"-type nanometric UCA based on mesoporous SiO_2 NPs with two contributing interfaces.[17] This innovative design increases the scattering cross-section through a double-shell structure, resulting in double backscattering and ultimately improving the contrast of ultrasonic imaging. The collaboration of these two shells in achieving the largest scattering cross-section is the key to the improved imaging efficiency. There is a negative correlation between the distance separating the two convex layers and both scattering cross-section and echogenic intensity. Smaller layer spacing results in a larger scattering cross-section and amplified scattering intensity. Based on this assumption, transforming the double-layer structure into a multi-layer configuration by introducing small NPs into the inner surface of NBs, so as to minimize the layer spacing, has the potential to maximize scattering intensity within limited dimensions.

SiO_2 NPs are common inorganic materials with natural echogenic properties, and they have recently been proposed as UCAs for CEUS due to the differences in acoustic impedance generated at the interface between tissues and rigid SiO_2 surfaces.[17,29–32] SiO_2 NPs also assure prolonged stability with respect to nanobubbles because bubble lifetime is limited by gas diffusion kinetics, whereas solid particles do not suffer from such limitations. Preliminary studies on the acoustic behaviors of SiO_2 NPs have demonstrated that SiO_2 NPs with a diameter of about 330 nm are very promising for use in CEUS at conventional diagnostic frequencies. "Rattle"-type mesoporous SiO_2 NPs were also designed at a diameter about 200–300 nm.[17,18] In our study, SiO_2 NPs showed low echogenicity as compared to other NBs with the same concentration due to a much smaller diameter of about 80 nm, which was designed for the

purpose of modifying the configuration and facilitating pharmaceutical fabrication. Convincingly, the quantitative analysis of the CEUS TIC verified that IR783-SiO_2NPs@NB was superior to IR783-NB in enhancing contrast signal intensity at an equivalent bubble concentration, confirming that augmenting the scattering cross-section within the structure of a nanometric UCA would lead to an enhanced rate of utilization of ultrasound and improved imaging contrast, thus improving CEUS effectiveness. Furthermore, when a certain amount of SiO_2 NPs was loaded into one NB, on the one hand, they increased the scattering cross-section, and thus helped in reflecting the ultrasound signal of the NB, while on the other hand, they also increasing the overall concentration of SiO_2 NPs released when the bubbles burst, which continued to act as UCAs for a while. This could also explain the enduring CEUS capability of IR783-SiO_2NPs@NB.

The active targeting feature of IR783 is highlighted in the present study. Besides this, as an NIRF dye, IR783 can also provide a dual-mode imaging modality, as the results indicate. The integration of optical and ultrasonographic imaging provides complementary information-enhancing diagnostic accuracy, especially in terms of visualizing the tumor boundary and possible metastatic lymph nodes. Moreover, contrast agents possessing dual-modal imaging capabilities can obtain both cellular and tissue-level images, thereby exhibiting significant potential in the early diagnosis of tumor diseases.[33]

NBs can easily be modified to incorporate a range of functional elements through either binding to the external surface or incorporation inside the inner core, allowing them to cater to imaging or therapeutic strategies.[4,34] "Donut-type" IR783-SiO_2NPs@NB are promising for use in overcoming the bottleneck problem of low ultrasound utilization efficiency by introducing multiple reflecting interfaces into a single NB. The newly constructed IR783-SiO_2NPs@NB also hold potential in the following applications: i) porous SiO_2 NPs are preferential drug/gene-delivery vehicles, which could expand the drug-loading capacity of NBs; ii) the inherent thermosensitive property of the phospholipid shell makes it capable of maintaining encapsulation at physiological temperature and switching to an unstable state at a higher temperature, leading to membrane destruction and the release of SiO_2 NPs, which could favor controlled anti-tumor heat treatment. This type of stimuli-responsive nanomedicine can enhance the specificity of on-site theranostics, while also achieving a high level of tumor accumulation mediated by nanostructures and reduced toxicity to normal tissues;[35] (iii) the small, rigid, and near-spherical SiO_2 NPs are the most capable of reaching antigen-presenting cells, and they induce a strong immune response in tumor immunotherapy triggered by thermal ablation.[36]

Conclusions

In this study, we fabricated hollow SiO_2 NPs and coated them with lipid membranes labeled with IR783 to create "donut-type" nanoscale UCA, designated as IR783-SiO_2NPs@NB. These demonstrated a uniform size, exceptional stability, and high biocompatibility. More significantly, owing to the robust tumor-targeting capacity conferred by IR783 and its multi-scattering structure, IR783-SiO_2NPs@NB exhibited a pronounced CEUS imaging capability and a relatively prolonged contrast duration for solid tumors. Therefore, this represents a novel approach to optimizing the contrast enhancement capability of NBs on a confined nanometer scale, and it offers new possibilities for the reformation of the structural design of UCAs.

Abbreviations

ANOVA, analysis of variance; AUC, area under the curve; BSC, backscattering coefficient; CCK-8, cell counting kit-8; CEUS, contrast-enhanced ultrasound; CLSM, confocal laser scanning microscope; DPPC, 1.2-dipalmitoyl-sn-glycero -3-phosphocholine; DSPE-PEG 2000, 1.2-distearoyl-sn-glycero-3-phosphoethanolamine-N- (methoxy (polyethylene glycol)-2000); EE, efficiency of encapsulation; EPR, enhanced permeability and retention; H&E, hematoxylin and eosin; MB, methylene blue; MI, mechanical index; NBs, nanobubbles; NIRF, near-infrared fluorescent; NPs, nanoparticles; PBS, phosphate-buffered saline; PI, peak intensity; ROI, region of interest; SD, standard deviation; SEM, scanning electron microscopy; TEM, transmission electron microscope; TEOS, tetraethyl orthosilicate; TIC, time–intensity curve; TTP, time to peak intensity; UCA, ultrasound contrast agents.

Data Sharing Statement

The data that support the findings of this study are available from the corresponding authors, Li Fan and Li Zhang, upon request.

Ethics Approval

All animal experiments complied with the National Research Council's Guide for the Care and Use of Laboratory Animals, and the animal experiments were approved by the Animal Care and Ethic Committee of Fourth Military Medical University (approval No. KY20213144-1).

Acknowledgments

We express our gratitude to Jikai Yin from Tangdu Hospital of Air Force Medical University for his assistance in conducting animal experiments. We thank for Department of Pharmaceutical Chemistry and Analysis of Air Force Medical University for providing us with experimental equipment.

Funding

The research was funded by the National Natural Science Foundation of China (Funder: Li, Fan) (No. 82171962), the National Natural Science Foundation of China (Funder: Li, Zhang) (No. 81571730), the Key Research and Development Program of Science and Technology Department of Shaanxi Province (Funder: Li, Fan) (No. 2022ZDLSF01-03), and the Key Research and Development Program of Science and Technology Department of Shaanxi Province (Funder: Li, Zhang) (No. 2023YBSF-497).

Disclosure

The authors declare no conflicts of interest.

References

1. Liang J, Qiao X, Qiu L, et al. Engineering versatile nanomedicines for ultrasonic tumor immunotherapy. *Adv Sci*. 2024;11(3):e2305392. doi:10.1002/advs.202305392
2. Zhang G, Ye H, Sun Y, Guo Z. Ultrasound molecular imaging and its applications in cancer diagnosis and therapy. *ACS Sens*. 2022;7(10):2857–2864. doi:10.1021/acssensors.2c01468
3. Alphandéry E. Ultrasound and nanomaterial: an efficient pair to fight cancer. *J Nanobiotechnology*. 2022;20(1):139. doi:10.1186/s12951-022-01243-w
4. Andrews LE, Chan MH, Liu RS. Nano-lipospheres as acoustically active ultrasound contrast agents: evolving tumor imaging and therapy technique. *Nanotechnology*. 2019;30(18):182001. doi:10.1088/1361-6528/aafeb9
5. Duan L, Yang L, Jin J, et al. Micro/nano-bubble-assisted ultrasound to enhance the epr effect and potential theranostic applications. *Theranostics*. 2020;10(2):462–483. doi:10.7150/thno.37593
6. Fernandes C, Suares D, Yergeri MC. Tumor microenvironment targeted nanotherapy. *Front Pharmacol*. 2018;9:1230. doi:10.3389/fphar.2018.01230
7. Cai X, Jiang Y, Lin M, et al. Ultrasound-responsive materials for drug/gene delivery. *Front Pharmacol*. 2019;10:1650. doi:10.3389/fphar.2019.01650
8. Li C, Chang Y, Hsiao M, Chan M. Ultrasound and nanomedicine for cancer-targeted drug delivery: screening, cellular mechanisms and therapeutic opportunities. *Pharmaceutics*. 2022;14(6):1282. doi:10.3390/pharmaceutics14061282
9. Pasupathy R, Pandian P, Selvamuthukumar S. Nanobubbles: a novel targeted drug delivery system. *Braz J Pharm Sci*. 2022;58:e19608. doi:10.1590/s2175-97902022e19604
10. Cai W, Lv W, Meng L, Duan Y, Zhang L. The combined effect of nanobubble-ir783-hpph-affibody complex and laser on her2-positive breast cancer. *Int J Nanomed*. 2023;18:339–351. doi:10.2147/IJN.S387409
11. Yan F, Song Z, Du M, Klibanov AL. Ultrasound molecular imaging for differentiation of benign and malignant tumors in patients. *Quant Imaging Med Surg*. 2018;8(11):1078–1083. doi:10.21037/qims.2018.12.08
12. Yang H, Cai W, Xu L, et al. Nanobubble–affibody: novel ultrasound contrast agents for targeted molecular ultrasound imaging of tumor. *Biomaterials*. 2015;37:279–288. doi:10.1016/j.biomaterials.2014.10.013
13. Lea-Banks H, O'Reilly MA, Hynynen K. Ultrasound-responsive droplets for therapy: a review. *J Control Release*. 2019;293:144–154. doi:10.1016/j.jconrel.2018.11.028
14. Ramirez DG, Ciccaglione M, Upadhyay AK, Pham VT, Borden MA, Benninger RKP. Detecting insulitis in type 1 diabetes with ultrasound phase-change contrast agents. *Proc Natl Acad Sci*. 2021;118(41):e2022523118. doi:10.1073/pnas.2022523118
15. Riaz R, Waqar H, Ahmad NM, Abbas SR. Novel magnetic elastic phase-change nanodroplets as dual mode contrast agent for ultrasound and magnetic resonance imaging. *Polymers*. 2022;14(14):2915. doi:10.3390/polym14142915

16. Loskutova K, Grishenkov D, Ghorbani M. Review on acoustic droplet vaporization in ultrasound diagnostics and therapeutics. *Biomed Res Int*. 2019;2019:1–20. doi:10.1155/2019/9480193
17. Zhang K, Chen H, Guo X, et al. Double-scattering/reflection in a single nanoparticle for intensified ultrasound imaging. *Sci Rep*. 2015;5(1):8766. doi:10.1038/srep08766
18. Zhang T, Zheng Q, Xie C, et al. Integration of silica nanorattles with manganese-doped In2S3/InOOH to enable ultrasound-mediated tumor theranostics. *ACS Appl Mater Interfaces*. 2023;15(4):4883–4894. doi:10.1021/acsami.2c18095
19. Zahiri M, Taghavi S, Abnous K, Taghdisi SM, Ramezani M, Alibolandi M. Theranostic nanobubbles towards smart nanomedicines. *J Control Release*. 2021;339:164–194. doi:10.1016/j.jconrel.2021.09.032
20. Koo B, Liu Y, Abboud M, et al. Characterizing how size distribution and concentration affect echogenicity of ultrasound contrast agents. *Ultrasonics*. 2023;127:106827. doi:10.1016/j.ultras.2022.106827
21. Kee ALY, Teo BM. Biomedical applications of acoustically responsive phase shift nanodroplets: current status and future directions. *Ultrason Sonochem*. 2019;56:37–45. doi:10.1016/j.ultsonch.2019.03.024
22. Lv W, Shen Y, Yang H, et al. A novel bimodal imaging agent targeting her2 molecule of breast cancer. *J Immunol Res*. 2018;2018:1–10. doi:10.1155/2018/6202876
23. Zhou T, Cai W, Yang H, et al. Annexin v conjugated nanobubbles: a novel ultrasound contrast agent for in vivo assessment of the apoptotic response in cancer therapy. *J Control Release*. 2018;276:113–124. doi:10.1016/j.jconrel.2018.03.008
24. Fan L, Yang J, Leung KC, Song C, Li Q. Noninvasive real-time monitoring of local drug release using nano-au-absorbed self-decomposable sio2 carriers. *Nanoscale*. 2018;10(32):15332–15338. doi:10.1039/c8nr03782e
25. Pang C, Song C, Li Y, et al. The establishment and application studies on precise lysosome ph indicator based on self-decomposable nanoparticles. *Nanoscale Res Lett*. 2020;15(1):143. doi:10.1186/s11671-020-03367-0
26. Zhu L, Wang L, Liu Y, Xu D, Fang K, Guo Y. Caix aptamer-functionalized targeted nanobubbles for ultrasound molecular imaging of various tumors. *Int J Nanomed*. 2018;13:6481–6495. doi:10.2147/IJN.S176287
27. Shen Y, Lv W, Yang H, et al. Fa-nbs-ir780: novel multifunctional nanobubbles as molecule-targeted ultrasound contrast agents for accurate diagnosis and photothermal therapy of cancer. *Cancer Lett*. 2019;455:14–25. doi:10.1016/j.canlet.2019.04.023
28. Merillas B, Martín-De León J, Villafañe F, Rodríguez-Pérez MÁ. Optical properties of polyisocyanurate–polyurethane aerogels: study of the scattering mechanisms. *Nanomaterials*. 2022;12(9):1522. doi:10.3390/nano12091522
29. Ho Y, Wu C, Jin Q, et al. Superhydrophobic drug-loaded mesoporous silica nanoparticles capped with β-cyclodextrin for ultrasound image-guided combined antivascular and chemo-sonodynamic therapy. *Biomaterials*. 2020;232:119723. doi:10.1016/j.biomaterials.2019.119723
30. Cheng L, Liu Y, Zou B, Yu Y, Ruan W, Wang Y. Template-etching route to construct uniform rattle-type fe3o4@sio2 hollow microspheres as drug carrier. *Mater Sci Eng C*. 2017;75:829–835. doi:10.1016/j.msec.2017.02.105
31. Alphandéry E. Nanomaterials as ultrasound theragnostic tools for heart disease treatment/diagnosis. *Int J Mol Sci*. 2022;23(3):1683. doi:10.3390/ijms23031683
32. Cha BG, Kim J. Functional mesoporous silica nanoparticles for bio-imaging applications. *WIREs Nanomed Nanobiotech*. 2019;11(1):e1515. doi:10.1002/wnan.1515
33. Xiao X, Cai H, Huang Q, et al. Polymeric dual-modal imaging nanoprobe with two-photon aggregation-induced emission for fluorescence imaging and gadolinium-chelation for magnetic resonance imaging. *Bioact Mater*. 2023;19:538–549. doi:10.1016/j.bioactmat.2022.04.026
34. Jose AD, Wu Z, Thakur SS. A comprehensive update of micro- and nanobubbles as theranostics in oncology. *Eur J Pharm Biopharm*. 2022;172:123–133. doi:10.1016/j.ejpb.2022.02.008
35. Li H, Feng Y, Luo Q, et al. Stimuli-activatable nanomedicine meets cancer theranostics. *Theranostics*. 2023;13(15):5386–5417. doi:10.7150/thno.87854
36. Benne N, van Duijn J, Kuiper J, Jiskoot W, Slütter B. Orchestrating immune responses: how size, shape and rigidity affect the immunogenicity of particulate vaccines. *J Control Release*. 2016;234:124–134. doi:10.1016/j.jconrel.2016.05.033